https://doi.org/10.5194/egusphere-2024-174
Preprint. Discussion started: 12 February 2024

Thunderstorm characteristics with lightning jumps and dives in satellite-based nowcasting

Felix Erdmann[1] and Dieter R. Poelman[1]

[1]Royal Meteorological institut of Belgium (RMI), Av. Circulaire 3, 1180 Uccle, Belgium

Correspondence: Felix Erdmann (felix.erdmann@meteo.be)

Abstract. The first Meteosat Third Generation (MTG) satellite was launched in December 2022. Its high resolution Flexible Combined Imager (FCI) in combination with the Lightning Imager (LI) herald a new period for geostationary (GEO) weather observations over Europe, Africa, and adjacent regions. Similar instruments are already operational over the U.S., with the Advanced Baseline Imagers (ABIs) and the Geostationary Lightning Mappers (GLMs). The objective of this study is to gain a deeper understanding of GEO data, with a specific emphasis on sudden increases in a storm's lightning activity, referred to as lightning jumps (LJ), and decreases, known as lightning dives (LD), as observed from a geostationary orbit. ABI-based cloud characteristics of thunderstorms are analyzed while storms are categorized by whether they produced LJs, LDs, or severe weather. It is found that the storms with LJs and/or LDs feature overall similar characteristics as the severe thunderstorms. Those storms typically feature elevated, colder cloud tops, more and stronger overshooting tops (OTs), consequently leading to more structured updrafts. As a result, these storms tend to generate higher convective rain rates (CRRs) on average compared to storms lacking LJs, LDs, and those categorized as non-severe. In particular, thunderstorms experiencing multiple LJs throughout their lifecycle exhibit the most and strongest OTs, signifying highly organized updrafts, extremely cold cloud tops, and highest CRRs. Considering the characteristics mentioned above, these storms, especially those featuring multiple LJs and LDs during their lifecycle, are of particular interest for nowcasting potentially dangerous weather phenomena.

1 Introduction

Thunderstorms have the potential to give rise to hazardous weather phenomena like strong winds, large hail, flash floods, and tornadoes. A thunderstorm, as its name implies, is defined as a cloud system that produces lightning and thunder. Hence, lightning observations can be used to locate these deep convective systems.

Each storm has its unique lightning characteristics with certain peaks and downs in the lightning activity during the lifecycle of the storm. Quantifying the changes in the lightning activity means analyzing the time series of the flash rate (FR) of the storm cell. Rapid increases in the FR are referred to as lightning jumps (LJs) as coined by Williams et al. (1999). The opposite behavior, a sudden decrease in the FR is termed a lightning dive (LD). Previous studies (e.g., Rudlosky and Fuelberg, 2013; Williams et al., 1999; Goodman et al., 1988) found relations between the occurrences of LJs and severe weather making LJs a potential tool for nowcasting severe weather. LJs could be correlated to hail events (e.g., Ni et al., 2023; Nisi et al., 2020; Wapler, 2017; Mikuš Jurković et al., 2015), tornadoes (e.g., Rudlosky and Fuelberg, 2013; Steiger et al., 2007a, b), severe

https://doi.org/10.5194/egusphere-2024-174
Preprint. Discussion started: 12 February 2024

wind events (e.g., Pandit et al., 2023), and also supercell development (Stough et al., 2017). Schultz et al. (2017) found that LJs result from an intensification of the mixed-phase updraft that also benefits the severe weather production.

Total, i.e., cloud-to-ground (CG) and inter- and intra-cloud (IC), lightning observations appear to be beneficial for nowcasting severe weather compared to using solely CG records (Schultz et al., 2011). The new generation of geostationary (GEO) satellites carries imagers to map the total lightning activity from space. The Geostationary Lightning Mapper (GLM, Goodman et al., 2013; Mach, 2020) provides coverage over the Americas and adjacent oceans, while the Meteosat Third Generation Lightning Imager (MTG-LI, EUMETSAT, 2021b; Dobber and Grandell, 2014) observes, among others Europe, Africa, and the Atlantic. In addition to the GEO lightning data, the new generation of GEO imagers such as the American Advanced Baseline Imager (ABI, NASA, 2022) and the MTG Flexible Combined Imager (FCI, EUMETSAT, 2021a) has seen improvements as well, featuring higher resolution and additional channels, i.e., wavelengths. ABI and GLM provide useful information for nowcasting thunderstorms (Cintineo et al., 2022; Leinonen et al., 2022; Chinchay, 2023). GLM lightning observations have demonstrated potential in the nowcasting of precipitation (with a determination coefficient of approximately 0.6), with limitations in accurately predicting high-intensity rain rates and accumulations (Bourscheidt and Ramos, 2023). Thiel et al. (2020) discriminates between convective and stratiform precipitation by analyzing GLM flash size and frequency. The findings indicate that the most frequent and smallest GLM flashes are associated with the coldest and highest ABI cloud tops (CTs), as well as with overshooting tops, i.e., signatures of strong convective updrafts.

Different approaches to automatically detect LJs were optimized through verification of the algorithm against the presence of severe weather (Gatlin and Goodman, 2010; Schultz et al., 2009, 2011, 2016; Erdmann and Poelman, 2023). However, most LJ algorithms were tuned based on ground-based lightning mapping array (LMA) data. Curtis et al. (2018) and Murphy and Said (2020) suggest that LJs found for GLM do not resemble LJs identified with LMAs as the former are less correlated to radar observations. Erdmann and Poelman (2023) optimized the LJ detection specifically for GLM lightning records in the central and eastern contiguous United States (CONUS). However, the LJs detected by GEO satellites have not yet been studied in detail and their significance has yet to be understood.

This present study continues the work of Erdmann and Poelman (2023) and should help understanding the GEO LJs and LDs better. The objective is to perform an extensive statistical analysis of thunderstorms, LJs and LDs, and the related cloud characteristics as observed from satellites. Thunderstorms are then categorized by the presence of LJs, LDs, and/or severe weather reports. Hence, thunderstorms with and without LJs (LDs, severe weather, respectively) can be compared to identify similarities and differences in the satellite-based cloud characteristics. Some previous studies conducted a similar kind of analysis for the LMA-based LJs. Chronis et al. (2015) found that storms with LJs are more organized, more intense, last longer, and exhibit more consistent lightning activity than storms without LJs. This finding was confirmed by Rigo and Farnell (2022) in particular for storms with multiple LJs. LJs could also be related to heavy precipitation events (e.g., Farnell and Rigo, 2020; Wu et al., 2018). The present study aims to determine whether comparable findings and conclusions emerge when utilizing GLM-based LJs and LDs.

https://doi.org/10.5194/egusphere-2024-174
Preprint. Discussion started: 12 February 2024

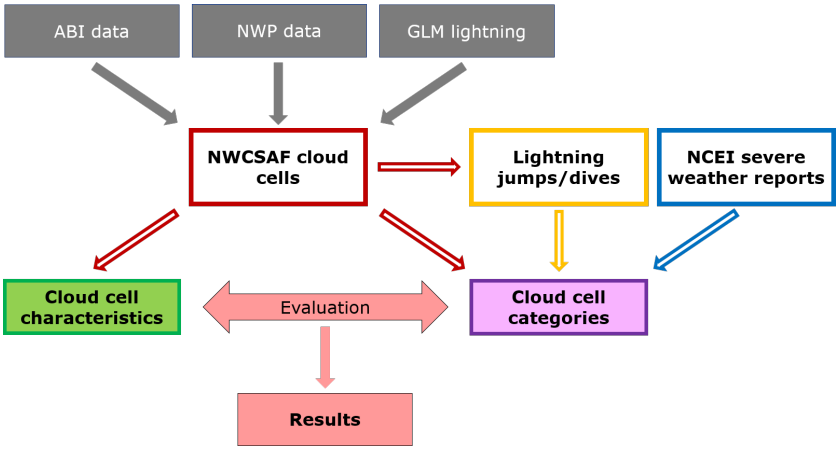

Figure 1. Relations between tools and data of this study.

Section 2 provides information on the datasets and outlines the data processing steps undertaken to derive the results. This encompasses thunderstorm identification, cloud cell tracking, and the detection of LJs and LDs. The subsequent sections, Section 3 and Section 4, delve into the description and discussion of the obtained results.

2 Data and Methods

The EUMETSAT satellite application facility (SAF) for nowcasting (NWC) has developed the central software package for this study (Section 2.1). The main source of data is the Geostationary Operational Environmental Satellites R-Series (GOES-R) 16 (former GOES-East) with its ABI and GLM instruments (Section 2.4). Figure 1 introduces the tools and data sources and their relations to each other. Dark grey data is ingested into the NWCSAF software that identifies cloud cells (red) and their satellite-based characteristics (green). Every cloud cell maintains a record of the FR history, allowing the implementation of the LJ/LD detection algorithm (Section 2.6, yellow). LJs/LDs in combination with the severe weather reports (Section 2.3, blue) are used to categorize the cloud cells (purple). The results reveal the characteristics of the different cloud cell categories.

2.1 NWCSAF nowcasting software and the RDT package

This work uses identical datasets and software package as in Erdmann and Poelman (2023). Hence, the software package and study periods are briefly introduced below, with more comprehensive details available in Erdmann and Poelman (2023).

The NWCSAF nowcasting software (EUMETSAT, 2022) is a comprehensive nowcasting tool based on satellite data as the prime source of information. NWCSAF v2018.1 (García-Pereda and coauthors, 2019) is used with implementation of technical changes in common modules and on convection products, along with the incorporation of a GLM data reader. This study ingests GOES ABI data (Section 2.4) standard scan with 10minute update cycle as necessary input. To enhance the quality of specific

https://doi.org/10.5194/egusphere-2024-174
Preprint. Discussion started: 12 February 2024

Table 1. Study periods and the number of analyzed thunderstorms (full trajectories) in the CONUS per period (excluding the spin-up time of 3h and instrument downtime).

Period	Number of storms
Jan 10-11, 2020	844
Feb 04-06, 2020	852
Jun 02-10, 2020	11256
Aug 14-16, 2020	5414
Nov 24-25, 2020	564
Jan 25-16, 2021	815
Feb 13-15, 2021	352
Apr 08-10, 2021	1313
Aug 30-31, 2021	3563
Overall	24973

products, especially in cloud cell detection and tracking, data from the European Centre for Medium-Range Weather Forecasts (ECMWF) numerical weather prediction (NWP) and GLM lightning are provided as optional input.

The NWCSAF software is equipped with various modules. The Rapid Developing Thunderstorm Convective Warning (RDT-CW) module (Autones et al., 2020) provides convective cell detection, tracking, and characterisation. The object-oriented approach can effectively differentiate between convective and non-convective cloud cells, and track the convective cells through image recognition, identification of known patterns, and statistical models. The RDT-CW provides outputs for each cell, including the cell contour, various physical cloud characteristics (as detailed in Section 2.5), information about brightness temperatures (BTs) and reflectances, convective rain rates (CRR), and the GLM flash rate (FR).

2.2 Study days

Study days are selected based on the following aspects: (i) There is a spinup for each NWCSAF software run of 3 hours as a trade-off between included data and negative effect on RDT during the beginning of the run. Hence, selected periods of more than 24 consecutive hours are prefered for efficiency. (ii) Each period should contain storms with different severe weather types ensuring a minimum of two among wind, hail, and tornado reports during the period's duration. (iii) The overall dataset should cover different seasons. (iv) GOES ABI and GLM data must be available. During our selected study days (Table 1), there was one important GOES-16 downtime from 03 Jun 17:00UTC to 04 June 01:30UTC.

It should be noted that only thunderstorms are analyzed that are defined as RDT cloud cells with GLM lightning activity. This studies aims at understanding the meaning of LJs and LDs for thunderstorm characteristics. RDT cloud cells without lightning activity are not further studied as they are stratiform phenomena, shallow convection, or cells during their early development or dissipation phase. Such cells generally give rise to weaker weather phenomena compared to major thunderstorms.

https://doi.org/10.5194/egusphere-2024-174
Preprint. Discussion started: 12 February 2024

2.3 National Centers for Environmental Information (NCEI) severe weather reports

The NCEI weather database collects reports of human observers to archive the frequency and impact of significant weather events in the U.S. that may cause loss of life, injuries, significant property damage, and/or disruption to commerce (NCEI-NOAA, 2020). The reports are validated by experts, hence, there is a quality control for the reports within the database. The reported events encompass a variety of types, ranging from severe weather events such as tornadoes, large hail, and thunderstorm winds, to extreme temperatures and rare, unusual weather phenomena. This study uses the severe weather reports indicated as tornado, large hail, and thunderstorm winds for the study periods introduced in Section 2.2.

A database scan (DBSCAN) algorithm (scikit-learn developers, 2007-2022) clusters all reports of the same type (i.e., tornado, hail, wind) that occurred within $10\mathrm{km}$ and $6\mathrm{minutes}$ (Erdmann and Poelman, 2023; Schultz et al., 2016). The cluster of reports, that is created, is called a severe weather event, and the time and location of the event correspond to the first report of the event. To allocate the severe weather events to RDT cloud cells, cloud cells are considered at the exact time of a weather event. Therefore, the RDT cells are shifted using their motion vectors. An NCEI event belongs to a cloud cell if it is found within the cloud cell contour at the time of the event. For NCEI events that do not fall inside any cloud cell contour, a distance of $50\mathrm{km}$ around the event is also considered to assign it to the closest RDT cloud cell within that radius. As a result, RDT cloud cells receive an additional attribute indicating whether they produced a tornado, hail, and/or wind report.

2.4 ABI and GLM data

ABI on GOES-R satellites observes the Western Hemisphere's weather, oceans and environment. The passive multichannel radiometer has 16 different spectral bands including two visible channels (at 0.5- and 1.0-km resolution), four near-infrared channels (at 1.0-km resolution), and ten infrared channels (at 2-km resolution) with on-orbit calibration. Each channel views specific aspects of the atmosphere or surface such as trees, water, clouds, moisture or smoke (NASA, 2022) providing unique information. Several products can be deduced including cloud top details such as height and phase, storm motion vectors, radiation products, land and sea temperatures, surface type, albedo, aerosol information, and fire and volcanic ash characterization. Applications include the monitoring of cloud formation, tracking severe weather, assessing fire, smoke, and air quality, as well as understanding ocean dynamics.

Only GOES-16's ABI is used here. Although this study analyses the western and central CONUS, where the ABI rapid scan is available, ABI standard scan with updated images every $10\mathrm{minutes}$ is used, with the region limited to the CONUS. This aids in efficiently running the NWCSAF software and reducing the data volume.

GLM features optical detection of the light emitted by lightning, which is visible on the cloud top or edges. It monitors the total lightning activity from GEO orbit with narrow-band sensitivity of $1\mathrm{nm}$ within the $777.4\mathrm{nmOnlyGOES}-16'\mathrm{sABIisusedhere}.$ oxygen band. The variable pitch pixel charge coupled device (CCD) reduces the effect of increasing pixel size towards the edge of the field of view (FoV). Hence, pixels measure $8\mathrm{km}$ nadir and $14\mathrm{km}$ at the edge of the FoV (Goodman et al., 2013). GLMs wide angle lense covers nearly the full disk (1372×1300 pixels). The primary detected elements are single illuminated pixels, referred to as events. Adjacent events of the same $2\mathrm{ms}$ time frame form a group. Groups are clustered to flashes by a weighted

https://doi.org/10.5194/egusphere-2024-174
Preprint. Discussion started: 12 February 2024

euclidean distance (WED) approach with 16.5km latitude and longitude and 0.33s temporal constraints (Mach, 2020). The impact of the GLM performance and variations of it over the CONUS are discussed in Appendix A. GLM flashes are ingested into the NWCSAF software. RDT then assigns the GLM flashes to the cloud cells, whose position relative to the flash radiance-weighted centroid is checked at the exact time the GLM flash occured. The software outputs the 1-minute time series of the flash rate (FR) for each cloud cell.

2.5 Thunderstorm characteristics and the normalization

In total, this study analyzes 26 thunderstorm characteristics (Table 2) that are deduced from ABI channels directly (i.e., brightness temperature [BT], BT difference [BTD] and reflectance) or provided by the RDT software based on ABI observations (e.g., rain rates and overshooting tops [OTs]). These characteristics are expected to identify a thunderstorm, and a comparison should be made across different thunderstorm categories. To facilitate the comparison and illustration of the results, the characteristics are normalized and then plotted in the final results sections (Section 3.2.2 and Section 3.2.3). The normalization uses Equation (1). It is important to note that the normalization uses the overall minimum and maximum of all analyzed thunderstorms, not the minimum and maximum of one thunderstorm category. This global normalization still allows for comparing statistics of the normalized categories. The range of 0 to 1 indicates whether a certain characteristic received low or high values for the analyzed category relative to all other thunderstorms.

$$x_n = \frac{x - min(X)}{max(X) - min(X)} \tag{1}$$

with x_n the normalized characteristic ranging from 0 to 1, x the characteristic for the analyzed thunderstorm category in physical units, X the population of x (i.e., including x of all analyzed thunderstorms), and $min(X)$ and $max(X)$ representing the population overall minimum and maximum, respectively.

2.6 Lightning jumps and lightning dives

Erdmann and Poelman (2023) optimized the LJ algorithm for GLM lightning records. There are two LJ detection algorithms that are recommended: (i) the flashes per area LJ algorithm (FRarea) that is a modification of the widely used σ LJ algorithm (Gatlin and Goodman, 2010; Schultz et al., 2009) and (ii) the relative increase level (RIL) algorithm.

Both algorithm types an FR activation criterion (FR threshold) implying that a specific FR level is required for a LJ to be considered possible. The FRarea LJ algorithm first smoothens and normalizes the FR to obtain a 2-minute averaged FR. The normalization is done per area by dividing the FR by the RDT cloud cell area of that specific time. Then, the discrete time derivative of this normalized 2-minute FR, DFRDT, is calculated. The σ value is obtained from the standard deviation of the DFRDT of the previous 5 (i.e., not including the most recent DFRDT) 2-minute time steps. The ratio of the most recent DFRDT to σ is called the σ level and serves as the LJ detection threshold. If the σ level exceeds a given threshold, a LJ is detected. This study uses the FRarea LJ algorithm with FR threshold of 15 and σ level of 1.0, as recommended by Erdmann and Poelman (2023).

https://doi.org/10.5194/egusphere-2024-174
Preprint. Discussion started: 12 February 2024

Table 2. Thunderstorm (TS) characteristics.

Characteristic	Description
avg T	BT average for cells of the trajectory
min T avg	minimum of the cell-averaged BTs for the trajectory
cell area	maximum area of a cell in the trajectory
vertical grad(T)	average vertical temperature gradient (absolute) of cells in the trajectory
vertical cooling rate	average change (inverted[1]) in the minimum temperature of the cell and the previous cell in the trajectory
min pressure (top)	minimum pressure of any CT pixel for trajectory
pressure trend (top) max	maximum for the trajectory in change (inverted) of CT pressure for a cell and the previous cell
max CRR	maximum convective rain rate for cells of the trajectory
mean CRR	average over all convective rain rates of the trajectory
median CRR	median from all convective rain rates of the trajectory
overshoot count max	maximum number of OTs for one cell of the trajectory
overshoot DT max	maximum IR11.2 BTD between pixels of the OT and the surrounding pixels for cells of the trajectory
cloud water fraction	fraction of liquid water ABI pixels to mixed-phase and pure ice pixels.
cloud ice fraction	fraction of pure ice ABI pixels to mixed-phase and liquid water pixels
cloud ice-to-water	fraction of pure ice ABI pixels to liquid water pixels.
IR1.6(max_refl) avg	average over the maximum reflectance in IR1.6 channel for cells of the trajectory
IR2.2(max_refl) avg	average over the maximum reflectances in IR2.2 channel for cells of the trajectory
IR3.9(min_BT) avg	average over minimum BTs in IR3.9 channel for the cells of the trajectory
WV6.2(min_BT) avg	average over minimum BTs in WV6.2 channel for the cells of the trajectory (upper level water vapor)
WV7.3(min_BT) avg	average over minimum BTs in WV7.3 channel for the cells of the trajectory (mid-level water vapor)
IR8.4(min_BT) avg	average over minimum BTs in IR8.4 channel for the cells of the trajectory
IR12.3(min_BT) avg	average over minimum BTs in IR12.3 channel for the cells of the trajectory
WV6.2-WV7.3(p90) max	maximum of the 90th percentiles of WV6.2-WV7.3 BTDs for the cloud cells of the trajectory
WV6.2-IR11.2(p90) max	maximum of the 90th percentiles of WV6.2-IR11.2 BTDs for the cloud cells of the trajectory
IR8.4-IR11.2(p90)	average over the 90th percentiles of IR8.4-IR11.2 BTDs for the cloud cells of the trajectory
IR12.3-IR11.2(p90)	average over the 90th percentiles of IR12.3-IR11.2 BTDs for the cloud cells of the trajectory

160 LDs are obtained by the same algorithm when using negative σ levels. The CSIs of the LD algorithms are initially calculated when verifying NCEI weather events for all analyzed thunderstorms (not shown), with the same verification method as for the LJs in Erdmann and Poelman (2023). The applied LD algorithm with highest CSI makes use of the FRarea algorithm with FR threshold of 10 and σ level of -1.0.

https://doi.org/10.5194/egusphere-2024-174
Preprint. Discussion started: 12 February 2024

3 Results

The thunderstorm categories are determined based on the detected LJs, LDs, and the NCEI severe weather events (Section 3.1). The findings discussed further analyze ABI-based cloud characteristics to comprehend the significance of GLM LJs and LDs: initially focusing on selected characteristics for different thunderstorm categories (Section 3.2.1), followed by a detailed examination of specific thunderstorm categories.

3.1 Thunderstorm categories

Thunderstorms are categorized based on the presence and absence of LJs, LDs, and NCEI severe weather events. A total of 24 thunderstorm categories emerge from this process. Table 3 presents those and also shows the number of thunderstorm trajectories in each category. The vast majority of thunderstorms does not produce a LJ (95.9 %), a LD (91.4 %), and/or severe weather (96.1 %). A thunderstorm can produce more than one type of severe weather (the sum of withTornado, withHail, and withWind is greater than the number of severe TSs). All storms with a LJ also had a LD with the current configuration and detection algorithms proved by an equal number of storms in the two categories withLJ (1031) and withLJ and LD (also 1031, see Table 3). There are storms with LJs and/or LDs that did not produce severe weather (59.9 % and 71.9 %, respectively). There are also severe thunderstorms without LJs (57.4 %) and/or LDs (38.0 %). Hence, the categories withLJ, withLD, and withNCEI show some overlap while each category also samples a significant portion of standalone storms. In the following, it is investigated whether the storms would sill show similarities in their characteristics so that the LJs and LDs can be useful for nowcasting severe weather. LJs and/or LDs might indicate that a storm has the ingredients to produce severe weather whereas other factors might play a role to eventually decide whether a storm turns severe or not.

3.2 LJs, LDs, severe weather and the cloud cell characteristics

The thunderstorm trajectories are categorized based on the presence and absence of LJs, LDs, and NCEI severe weather events during the lifecyle of the storm. The key questions to be answered are (i) Do thunderstorms with LJs and/or LDs feature particular characteristics?, (ii) How do the severe thunderstorms compare to the thunderstorms with LJs and/or LDs?, and (iii) Is the number of LJs or LDs important?

3.2.1 Comparison of thunderstorm categories

The comparison of all 24 thunderstorm categories (Table 3) includes all 26 thunderstorm characteristics (Table 2). This section summarizes the most important findings going through the characteristics. Figure 2 illustrates the comparison of three selected characteristics for all categories: (a) maximum CRR, (b) cloud ice fraction, and (c) WV6.2-IR11.2 BTD. These three selected characteristics represent physical and typical satellite characteristics.

Cells with LJs, LDs, and/or severe storms have in general colder CTs than storms without LJs, LDs, and non-severe thunderstorms. Coldest CT temperature is found for the multiLJ (average about 204 K) and LJ & NCEI (average about 205 K) categories. The categories noLJ, noLD, noLJ & noLD, noNCEI, noLJ & noNCEI, and noLD & noNCEI feature the warmest

https://doi.org/10.5194/egusphere-2024-174
Preprint. Discussion started: 12 February 2024

Table 3. Thunderstorm (TS) categories and the number (n) of full trajectories in each category.

TS category (short name)	Number (n)
all	24973
with LJ (withLJ)	1031
with 1 LJ (singleLJ)	519
with multiple LJs (multiLJ)	512
without LJs (noLJ)	23942
with LD (withLD)	2136
with 1 LD (singleLD)	1464
with multiple LDs (multiLD)	672
without LDs (noLD)	22837
with LJ and LD (LJ & LD)	1031
without LJ and with LD (noLJ & LD)	1105
without LJ and without LD (noLJ & noLD)	22837
severe TS (withNCEI)	970
tornadic TS (withTornado)	79
with severe hail (withHail)	438
with severe wind (withWind)	645
non-severe TS (noNCEI)	24003
severe TS with LJ (LJ & NCEI)	413
severe TS without LJs (noLJ & NCEI)	557
non-severe TS with LJ (LJ & noNCEI)	618
non-severe TS without LJs (noLJ & noNCEI)	23385
severe TS with LD (LD & NCEI)	601
severe TS without LDs (noLD & NCEI)	369
non-severe TS with LD (LD & noNCEI)	1535
non-severe TS without LDs (noLD & noNCEI)	22468

CT temperatures (average of minimum BTs about 230 K). These findings are seen in the avg T, min T avg, and IR channel characteristics (not shown). The min pressure (top) agrees with the BTs, meaning the categories with the coldest CTs have the lowest CT pressure (average about 110-120 hPa). Highest average CT minimum pressure (about 210-220 hPa) is found for the 5 categories with the warmest CTs. The vertical grad(T) of a cell is influenced by both the tropospheric vertical temperature gradient and the vertical extent of the cloud. In general, the temperature decreases with height in the troposphere, and the temperature gradient is highest in the low levels and decreases with height. The vertical temperature gradient becomes 0 just above the tropopause and inverts to increasing temperature with height in the stratosphere. Hence, for shallow convection and clouds with lower CTs, there are slightly stronger vertical grad(T) than for the thunderstorms with CTs near the tropopause

https://doi.org/10.5194/egusphere-2024-174
Preprint. Discussion started: 12 February 2024

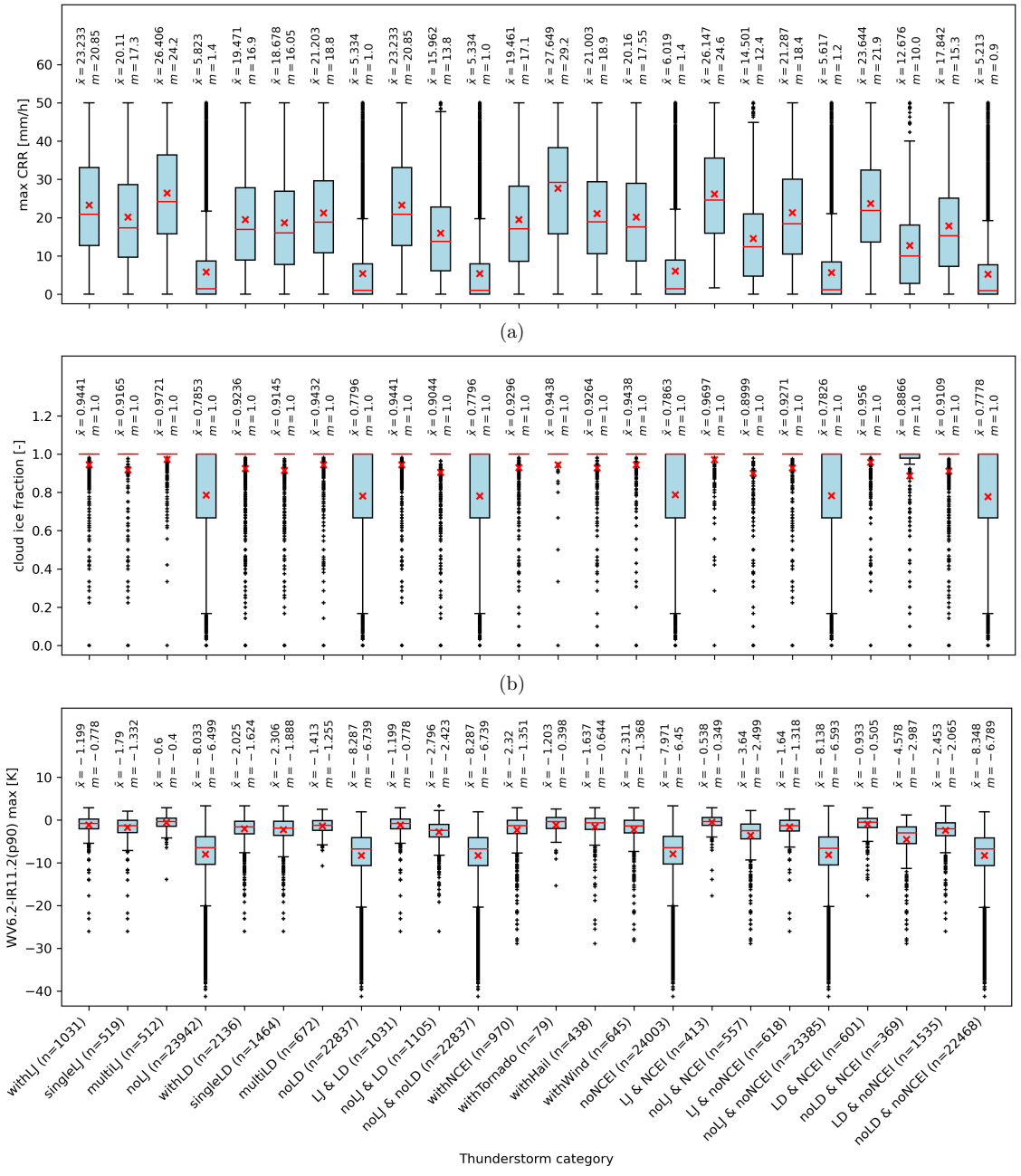

Figure 2. Distributions of (a) maximum estimated CRR during the cell lifecycle, (b) the fraction of pure ice pixels to mixed-phase and liquid water pixels (cloud ice fraction), (c) BTDs of WV6.2-IR11.2 as the maximum of the 90th percentiles BTD for each time step during the cloud cell lifecycle for the thunderstorm cell categories. $\bar{x}$ shows the mean, m the median for each category.

https://doi.org/10.5194/egusphere-2024-174
Preprint. Discussion started: 12 February 2024

(i.e., the categories with LJs and/or LDs and severe storms). This behavior also explains slightly lower vertical cooling rates for the thunderstorm categories with the highest CTs compared to the thunderstorms with lower average CTs.

The largest average cell areas occur for the thunderstorm categories multiLJ, withTornado, LJ & NCEI, and LD & NCEI (mean cell area of 9000-12000 $\mathrm{km2}$). On the opposite, the noLJ, noLD, and noNCEI storms cell area mean covers only about 1000 $\mathrm{km2}$. The distributions (not shown) also reveal that large cells are rare for the latter thunderstorm categories, however, there are also some large cells (cell area greater than 50000 $\mathrm{km2}$) without LJs, LDs, and/or NCEI reports. Such large cell area exist for all thunderstorm categories.

The speed of cell development, i.e., the pressure trend (top) max, does not show any tendency. Neither category contains cells that would grow more rapidly than thunderstorms in the other categories. The mean of the maximum rate of grows is about 6-8 $\mathrm{Pa/s}$.

The analysis of the CT phase (as satellite pixels) confirms the previous findings and shows that the cloud physics are in accordance with the BT measurements. Cloud water fraction is highest for the thunderstorms without LJs, LDs, and/or NCEI events (means of 0.15-0.16). Accordingly, cloud ice fraction (Figure 2b) shows the lowest mean values for these categories (0.71-0.72). Means for the categories withLJ, especially multiLJ, LJ & NCEI, and LD & NCEI are greater than 0.95, thus, almost 1. Cells in these categories consist on average of ice-phase ABI pixels only. Figure 2b also demonstrates that the variation among the severe weather types (tornado, hail, wind) is low and all feature high cloud ice fraction. It should be noted that the median of cloud ice fraction is always 1, for all categories. That is the case since thunderstorm cells are analyzed and there are always more than 50 $\%$ of ice pixels[2].

Overshooting tops (OTs) define a region of the cloud top that exceeds the surrounding cloud shield, often seen as a dome above an anvil. Sometimes OTs even break through the tropopause. OTs are usual transient features, so this study analyzes the maximum OT activity of each thunderstorm. OT development needs a strong force manifestated as a strong, persistent updraft in thunderstorms. The air gets accelerated vertically and can overshoot the level of thermal equilibrium. Hence, OTs are indicative of dynamical thunderstorm cells with strong updrafts that are usually well organized. Given that strong updrafts frequently play a crucial role in the formation of tornadoes and large hail, storms with these characteristics are especially significant for nowcasting. Most and strongest OTs occured in thunderstorms of the categories multiLJ, withTornado, withHail, LJ & NCEI, and LD & NCEI. The counts of OTs are higher in thunderstorms with LJs and/or LDs compared to the storms without LJs and LDs. Hardly any OTs are seen for the thunderstorms without LJs and/or LDs and the non-severe storms. It was expected to see more and stronger OTs, i.e., higher OT DT max, in the severe than the non-severe storms, and the same trend is found for the storms with LJs (LDs) compared to storms without LJs (LDs). Especially the multiLJ storms have OT counts and OT DT max above average, resembling the patterns observed in severe storms. There are severe storms without OTs, and the majority of them produced severe wind gusts. The withWind category of storms is less correlated to OTs than the other severe weather types.

CRRs are estimated by the RDT software. Statistics of the maximum CRR during the thunderstorm lifecycle are shown in Figure 2a. The storm categories noLJ, noLD, noCEI and combinations thereof exhibit noticeably the lowest max CRRs

[2]The median of cloud water fraction is always 0 for the same reason

https://doi.org/10.5194/egusphere-2024-174
Preprint. Discussion started: 12 February 2024

with mean values below 6 $\mathrm{mm/h}$ and median of less than 1.5 $\mathrm{mm/h}$. The highest max CRRs are observed for the categories withTornado (mean: 27.6 $\mathrm{mm/h}$), multiLJ (26.4 $\mathrm{mm/h}$), and LJ & NCEI (26.1 $\mathrm{mm/h}$). Thunderstorms with LDs have mean max CRR of 19.5 $\mathrm{mm/h}$, thus, somewhat lower than the storms with LJs (23.2 $\mathrm{mm/h}$) but similar compared to all severe storms (19.5 $\mathrm{mm/h}$). The category withTornado has significantly higher max CRR than hail and wind severe storms (Figure 2a). The results for the mean CRR and median CRR during the thunderstorm lifecycles lead to similar conclusions as the ones presented for the max CRR. Hence, the storms in the stated categories with high CRR produce significant amounts of rainfall throughout their entire lifecycle.

Both the WV6.2 and the WV7.3 channel exhibit the lowest BTs for the multiLJ and LJ & NCEI thunderstorms. Hence, the highest amount of upper and mid level water vapor is found for these two thunderstorm categories. The water vapor content affects the possibility of condensation, cloud formation, and directly influences the maximum amount of precipitation. High water vapor content means high amounts of water being stored in the atmosphere that could be released as precipitation. Thunderstorms that produced tornadoes and/or severe hail contain more water vapor in the mid and upper levels than the severe wind storms. In general, the results for water vapor content are consistent with the results for CRR, however, the tornadic storms with the highest CRRs of all categories stand out, although they may not possess the single highest water vapor content.

BTDs are commonly used in satellite science since they combine information from different channels. For example, IR11.2 alone gives information about the CT temperature, however, it does not tell anything about the clouds below. Combining IR11.2 and WV6.2 (Figure 2c) provides information about the CT and upper level water vapor content. BTDs as defined in this study (Table 2) have in general negative values for cloud cells. The BTD gets closer to 0 or becomes slightly positive for the deep convective clouds. Hence, the higher the BTD, the more organized the convection and the cloud cell. Mean BTDs are significantly higher for the thunderstorm categories with LJs, LDs, and/or NCEI reports. For example, the WV6.2-IR11.2(p90) max averages -2 K to -1 K for the categories withLJ, withLD, and withNCEI, and even above -1 K for the multiLJ, LJ & NCEI, and LD & NCEI thunderstorms (Figure 2c). The means for thunderstorm categories without LJs, LDs, and NCEI reports are in the range of -9 K to -8 K. Figure 2c illustrates that high negative BTDs below -20 K of WV6.2-IR11.2(p90) max are mainly found for the thunderstorms without LJs, LDs, and NCEI reports. These low BTDs indicate shallow convection. Hence, it is evident that the shallow convection rarely leads to LJs and/or LDs and severe weather.

Overall, thunderstorms with LJs and/or LDs feature similar characteristics as the severe thunderstorms. These storm categories show statistically more organized convection with stronger updrafts and higher CTs than the thunderstorms without LJs and LDs and the non-severe storms. In addition, the latter are less likely to produce high amounts of rain and, thus, less likely to cause dangerous flash floods. The multiLJ storms are found as the most organized ones, and potentially the most dangerous thunderstorms.

3.2.2 Non-LJ thunderstorms versus LJ storms and LD storms

The comprehensive comparison of thunderstorms with and without LJs and LDs, respectively, uses the normalized characteristics (Section 2.5). Figure 3 shows all characteristics for the thunderstorms (a) without, (b) with LJs, and (c) with LDs. The characteristics avg T, min T avg, IR8.4(min_BT) avg, and IR12.3(min_BT) avg all have significantly lower values for

https://doi.org/10.5194/egusphere-2024-174
Preprint. Discussion started: 12 February 2024

the storms with LJs than for storms without LJs (Figure 3 a and b, respectively). This difference is significant, as even the interquartile ranges (IQR) highlighted in blue in Figure 3 show no overlap. Lower values mean colder temperatures and higher CTs, which agrees with the results for min pressure (top). Thunderstorms with LJs cover also significantly more area than the thunderstorms without LJs. This could be related to the formation of large anvils for CTs near the tropopause. The on average lower CTs for the storms without LJs also explain the higher vertical grad(T) as the tropospheric temperature gradient usually diminishes towards the tropopause.

The thunderstorms with LJs have lower BTs for both WV6.2 and WV7.3 channels compared to storms without LJs (Figure 3a and b). In particular, the difference is more pronounced in the mid-level water vapor content (WV7.3) than in the difference observed in the upper level water vapor channel (WV6.2). The mid-level water vapor has a major influence on precipitation amounts. In consequence, max CRR, mean CRR, and median CRR are significantly higher for the thunderstorms with LJs than for non-LJ thunderstorms.

Mean and median OT count max equal 0.0 for thunderstorms without LJs, and even the IQR has 0 range (Figure 3a). Therefore, OTs occur as rare exceptions in the non-LJ storms, and they are more frequent for the thunderstorms with LJs (Figure 3b). The storms with LJs feature more persistent and stronger updrafts. It is often the case that graupel forms within the updraft regions, that can then collide with small ice crystals. That non-inductive charging is the major cloud electrification process in extratropical thunderstorms (e.g., MacGorman and Rust, 1998), thus, strong updrafts often cause an increase in the storm FR (see also Deierling and Petersen, 2008). As the updrafts also indicate organized convective cells, these storms manifest as deep convection. The BTDs WV6.2-WV7.3(p90) max and WV6.2-WV11.2(p90) max are in accordance with that theory as they yield higher values for the LJ storms compared to the non-LJ storms. Storms with LJs form in regions characterized by the highest levels of upper level moisture and evolve through the intensification of deep convection. BTDs of the IR channels yield similar values for the storms with and without LJs as all thunderstorms have a high percentage of CT glaciation (IR8.4-IR11.2). The cloud ice fraction confirms that the median for both storms with and without LJs is 1. Mean cloud ice fraction for the non-LJ storms is lower (0.79, Figure 3a) than for LJ storms (0.94, Figure 3b), however, the majority of the cloud is glaciated for all thunderstorms.

Figure 3(c) shows the normalized characteristics for the thunderstorms with LDs. It should be noted that the thunderstorms with LDs contain among others all the thunderstorms with LJs. The number of storm trajectories with LDs is about double the number of storm trajectories with LJs. Hence, half of the withLD storms have not been included in the withLJ analysis. These trajectories cause the differences seen in LJ (Figure 3b) and LD (Figure 3c) storms: The LJ storms have slightly colder CT temperatures and lower CT pressure, they cover a larger area, engender more likely high CRRs and consistently high amounts of rain, and produce on average more and stronger OTs than the thunderstorms with LDs. Therefore, the LJ detection has a stronger correlation to the most organized convection than the LD detection. LDs occured also in storms with weaker updrafts and lower CTs. LDs could still obtain similar CSI when verifying NCEI severe weather events (with the method of Erdmann and Poelman, 2023, not shown) since there are severe weather events that occur in shallow convection or storms that would not have the strongest updrafts (i.e., no OTs).

https://doi.org/10.5194/egusphere-2024-174
Preprint. Discussion started: 12 February 2024

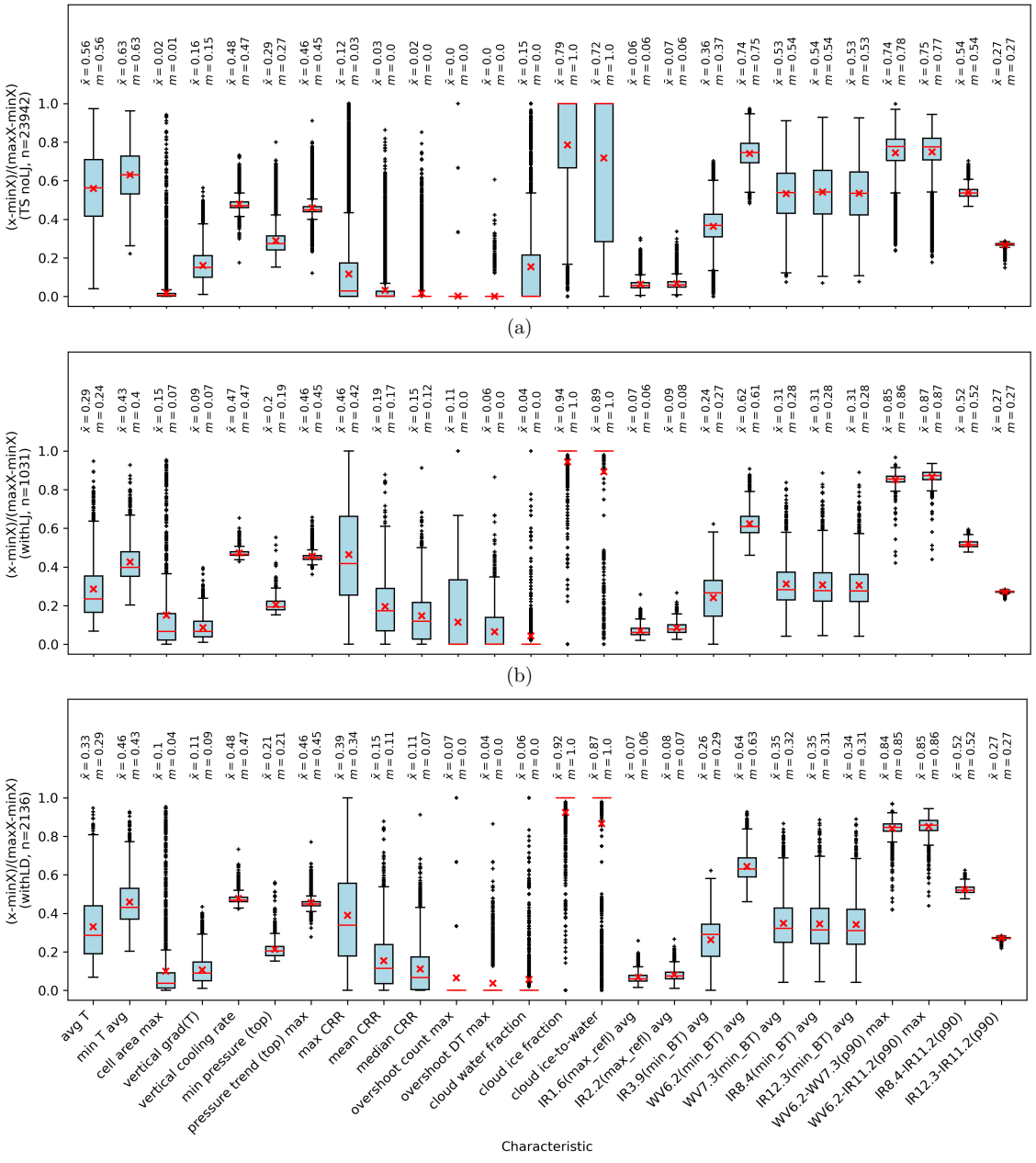

Figure 3. Normalized characteristics for (a) the thunderstorms (TS) without LJs and (b) the storms with LJs, and (c) the storms with LDs. $\bar{x}$ shows the mean, m the median for each characteristic.

https://doi.org/10.5194/egusphere-2024-174
Preprint. Discussion started: 12 February 2024

3.2.3 Single LJ versus multiple LJ storms

The previous sections compared storms with LJs to storms without LJs and to storms with LDs. Here, the specific meaning of multiple LJs for the characteristics of thunderstorms is pointed out by comparing these storms to the single LJ storms. Figure 4 presents the normalized characteristics for these two categories. This section puts emphasis on the differences that are found for characteristics of thunderstorms with multiple and single LJs. Multiple LJ storms (Figure 4b) have slightly colder and higher CTs than single LJ storms (Figure 4a). Thunderstorms with multiple LJs during their lifetime manifest the deepest convection. OTs are notably more frequent and significantly stronger in storms with multiple LJs compared to those with only a single LJ, as suggested by both the average values and the IQRs of OT count max and OT DT max in Figure 4. Strong, organized updrafts occur mostly within the multiLJ storms. However, the water vapor channels and BTDs yield similar values for the multiLJ and singleLJ storms. Both storm categories contain deep convective cells that form in similar environments. Hence, the updraft strength remains a major difference between multiLJ and singleLJ storms. The average (mean and median) CRR increases for the multiLJ relative to singleLJ storms. The max CRR of multiLJ storms clearly exceeds that of singleLJ storms. This implies that the storms with multiple LJs are more prone to experiencing the highest rain rates, posing an elevated risk of flash floods compared to storms with only one LJ (see also Figure 2a for CRR values). All these results for the GLM-based LJs agree well with Rigo and Farnell (2022) that analyzed LMA-based multi-LJ storms.

4 Discussion and final remarks

This work had the objective to understand lightning jumps (LJs) and lightning dives (LDs) identified from GLM lightning records. This analysis examines thunderstorm characteristics for storms with and without LJs and LDs, as well as for severe and non-severe thunderstorms. The NWCSAF nowcasting software provides GOES-16 ABI characteristics for tracked thunderstorm cells. Based on the storm flash rate (FR), the FRarea LJ and LD algorithms (Erdmann and Poelman, 2023) were applied to automatically detect LJs and LDs for each thunderstorm trajetory. LJs, LDs, and NCEI severe weather reports allow then the categorization of the thunderstorm trajectories so that storm categories are obtained for LJ and non-LJ, LD and non-LD, and severe and non-severe thunderstorms. All ABI characteristics can be compared across different categories. To summarize the findings, the questions posed at the beginning of the results section are addressed:

Do thunderstorms with LJs and/or LDs feature particular characteristics? The thunderstorms with LJs and/or LDs show statistically stronger vertical development with colder and higher cloud tops (CTs), and also higher convective rain rates (CRR) than storms without LJs and LDs. The cell size, overshooting top (OT) counts, and degree of cloud glaciation are above the average of all thunderstorms. Their overall characteristics resample the characteristics of the severe thunderstorms, thus, thunderstorms with LJs and/or LDs are more favorable of producing severe weather and heavy rain.

How do the severe thunderstorms compare to the thunderstorms with LJs and/or LDs? The severe storms often feature characteristics similar to the storms with LJs (and LDs). The tornadic storms appear as the most organized ones, most closely matched by the storms with multiple LJs.

https://doi.org/10.5194/egusphere-2024-174
Preprint. Discussion started: 12 February 2024

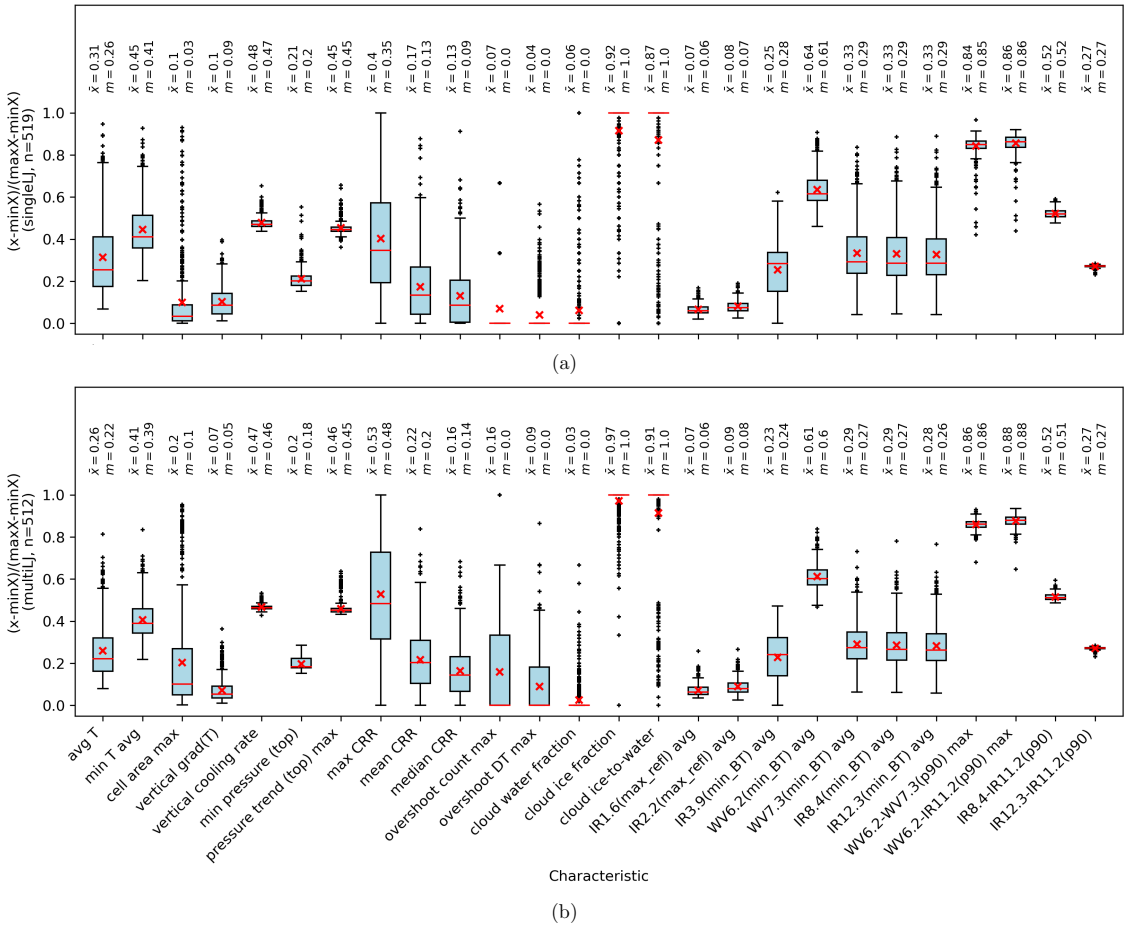

Figure 4. Normalized characteristics for (a) the storms with a single LJ and (b) the storms with multiple LJs during their lifecycle. $\bar{x}$ shows the mean, m the median for each characteristic.

Is the number of LJs or LDs important? Yes, this is specifically true for the LJs. Storms with multiple LDs showed similar vertical development and OTs as the storms with a single LD, with just slightly higher maximum rain rates. The multi-LJ storms, however, contain more organized and stronger updrafts (indicated by the OTs) than the single-LJ storms. In addition, they are more likely to produce the highest CRRs that might cause flash floods.

It should be mentioned that the results were similar with the use of other LJ and LD algorithms from Erdmann and Poelman (2023) such as the RIL algorithm. LDs could occur when the storms dissipate and the flash rate (FR) drops naturally due to the dissipation of the storm. An advanced LD detection algorithm that excludes the dissipation phase of the storm might gain better results for correlating LDs and severe weather.

The spring plus summer and the fall plus winter trajectories were separated to analyze the warm and cold season thunderstorms. The data includes about 21.5 and 3.5 thousand thunderstorms during the warm and cold season, respectively. It is noted

https://doi.org/10.5194/egusphere-2024-174
Preprint. Discussion started: 12 February 2024

that warm season LD-to-LJ ratio is 2.1, and in cold season 1.9. In warm seasons, storm cells with LJs exhibit a larger area compared to those in cold seasons. The LD storms do not show any difference in the cell area between the seasons. CT temperatures were similar during warm and cold season for thunderstorms with LJs, LDs, and/or severe thunderstorms. For the categories that include some shallow thunderstorms (i.e., those without LJs and/or LDs, non-severe storms), the CTs are about 5 to 10 K warmer during the warm than during the cold season. The minimum pressure at the top indicates lower pressure during the warm season compared to the cold season. This is attributed to the overall warmer atmosphere, and the natural cloud ceiling, i.e., the troposphere, being situated at higher altitudes. Since climatology causes this result, it is consistent for all thunderstorm categories. Hence, the tropopause is at different altitudes during warm and cold season but its temperature (i.e., temperature of the highest CTs) is similar. The average OT counts and OT DT max show no difference in cold and warm season for the LJ storms. Storms with LDs experienced a greater number of more intense OTs during the cold season compared to the warm season. Hence, LDs during the cold season, despite being less frequent and generally having lower FR, may be more significant for nowcasting than LDs observed in the warm season. The thunderstorms during both seasons produced similar max CRR. The higher mean and median CRR during the cold season suggest continuous precipitation associated with cold-season storms. These storms predominantly occur along air mass boundaries, involving large-scale lifting of air and resulting in widespread precipitation. Warm season storms can produce short, heavy showers but are less likely to produce a lot of rain during their entire lifetime. It is worth mentioning that winter tornadic storms, represented by only 25 trajectories, stand out due to their large cells, most and strongest OTs and highest max CRR. Tornadoes during the cold season formed only within exceptionally strong and well-organized storm cells, which presumably had low cloud base heights.

The most important finding of this study remains the behavior of thunderstorms that produced multiple GLM LJs during their lifecycle. These storms feature the strongest updrafts and highest cloud tops, and have all ingredients to produce severe weather and very high rain rates. Especially (though not exclusively) these storms should be closely monitored for weather advisory and weather warnings. GLM-based LJs have been observed to precede severe weather events by tens of minutes (Erdmann and Poelman, 2023) and may mean the first noticeable signature of developing weather hazards.

Code availability. Python 3.8 coding was used, with standard libraries and Matplotlib for the figures. The code was mainly developed during Felix Erdmann's PhD and as such is the property of the funders EUMETSAT and RMIB. Python code that is subject to active research and further studies cannot be made available. Parts of the code (Python scripts) are available from the corresponding author upon request.

Data availability. The NWCSAF software is available on the NWCSAF website (https://www.nwcsaf.org). ABI data are available online via NASA EARTHDATA (https://search.earthdata.nasa.gov/portal/idn/search?fi=ABI). GLM data are available online via NASA CLASS (https://www.avl.class.noaa.gov/saa/products/search?sub_id=0&datatype_family=GRGLMPROD&submit.x=22&submit.y=2). Access to ECMWF data requires a user account and access token. The NCEI weather reports are online (https://www.ncdc.noaa.gov/stormevents/).

https://doi.org/10.5194/egusphere-2024-174
Preprint. Discussion started: 12 February 2024

Appendix A: GLM flash detection efficiency impact

GLM performance depends on the nature of lightning itself, and also on cloud characteristics and thunderstorm development. The instrument performance can be assessed through comparison to other lightning locating systems (LLSs) via a relative detection efficiency (DE)[3]. GLM DE varies with the region within the field-of-view (Cummins, 2021; Blakeslee et al., 2020; Murphy and Said, 2020; Marchand et al., 2019). Technical aspects like the viewing angle and parallax play a role (Bruning et al., 2019). Furthermore, thunderstorm evolution and cloud characteristics influence GLM performance (Borque et al., 2020; Lang et al., 2020), and GLM DE seems to degrade during periods of overshooting tops (OTs). Zhang and Cummins (2020) reported in agreement with most of the previously cited studies, that GLM performs optimal for large, long lasting flashes. The GLM DE decreases during periods of very high flash rates or small flash sizes. As an optical instrument, GLM shows day-night DE differences: Overall, Cummins (2021); Zhang and Cummins (2020); Murphy and Said (2020); Marchand et al. (2019) suggest 10-15% higher DE at night than during daytime over the CONUS. (Bateman et al., 2021; Erdmann, 2020) found small differences in GLM day- and nightime DE due to the use of coarse criteria and a limited region, respectively. Nevertheless, the influence of GLM flash DE on LJ/LD detection and the results of this study are anticipated to be minimal, as demonstrated in Appendix A1.

A1 Impact of GLM flash DE on the detection of LJs

The dependency of GLM flash DE on the region is a systematic problem. Therefore, it is possible to analyze GLM observations in regions exhibiting different DE to assess the impact of GLM DE on the outcomes of this study. Based on Cummins (2021), a detection threshold of 3 fJ is used to separate U.S. states with lower (central and northern CONUS) and higher (southeast CONUS) GLM DE. Then, LJs have automatically been detected (Section 2.6) and verified using NCEI severe weather reports. Figure A1 displays the counts of LJs and NCEI severe weather reports for the region of higher (a,c) and lower GLM DE (b,d), respectively. The pixels of maximum LJ counts agree with the occurrence of severe weather. In some regions, LJ activity is highest where tornadoes occurred (e.g., southern Mississippi or Minnesota). In other regions (e.g., Louisiana) high LJ counts correlate with the local maximum in hail events. The high count of NCEI weather events around the Great Lakes and northeast CONUS mainly comes from wind reports that are less spatially correlated to the LJs compared to hail and tornadoes.

Overall, critical success index (CSI) yield similar skill in both regions when verifying the LJs with NCEI servere weather events (not shown). The correlation of LJs to NCEI reports does not depend on the different GLM flash DE. However, it was found that the number of false alarms, i.e., LJs that occurred independently of a severe weather events, could be reduced in the region of higher GLM DE if the LJ detection algorithm uses a higher FR threshold than for the full CONUS (see Section 2.6). It should be mentioned that this study considers the occurrences of LJs, not their strengths. LJ strengths and maximum flash rates may well be higher in the region of higher GLM flash DE, however, the number of LJs and their correlation to NCEI reports was little affected by the GLM flash DE.

[3]The relative DE expresses the ratio of lightning processes that are detected by the reference LLS and could also be detected by the evaluated LLS.

https://doi.org/10.5194/egusphere-2024-174
Preprint. Discussion started: 12 February 2024

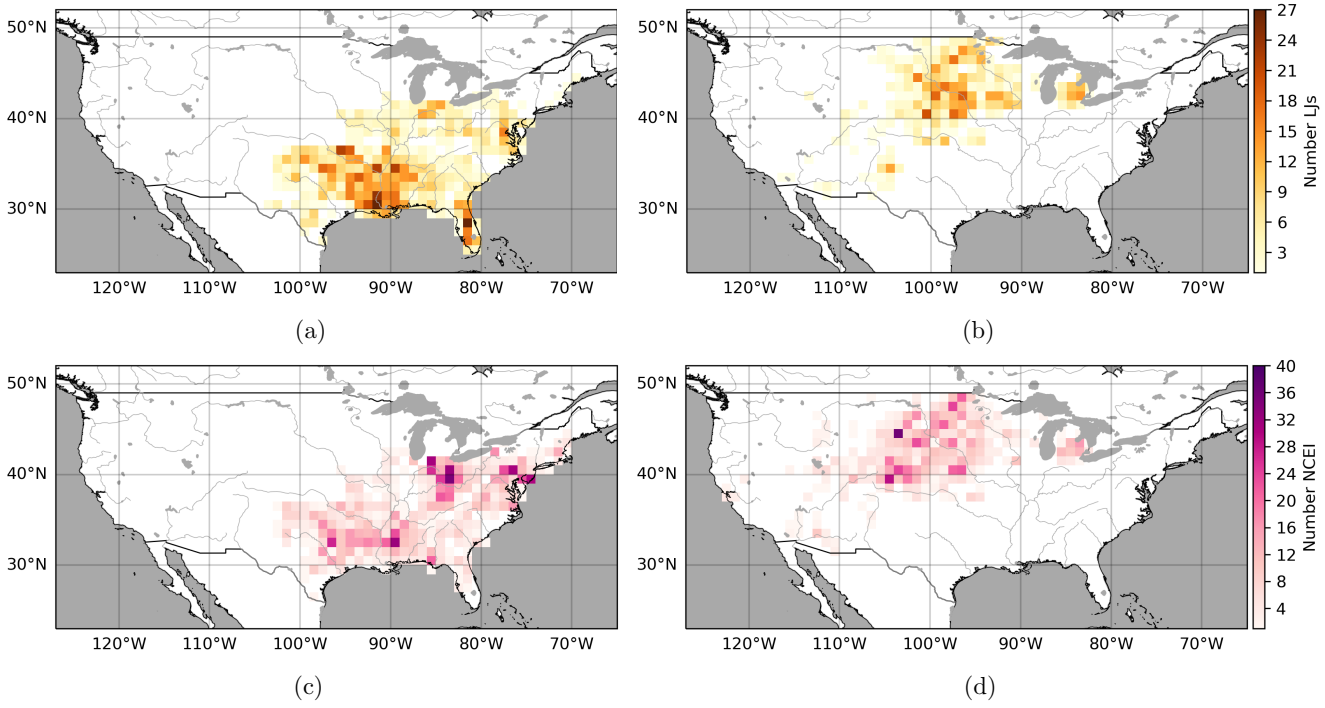

Figure A1. Number of (a,b) LJs, and (c,d) NCEI weather events (tornadoes, hail, wind) per 1×1 pixel in the region of (a,c) higher and (b,d) lower GLM DE.

A2 Thunderstorm cloud characteristics

There were, in total, 16155 and 8818 thunderstorms in the region of higher and lower GLM DE, respectively. Both regions contain a statistically relevant number of cases to analyze and compare the thunderstorm cloud characteristics. In particular, this section examines the characteristics of thunderstorms and investigates whether storms with LJ and/or LD exhibit distinct characteristics in the two regions. Main differences in the cloud characteristics occur due to the climatology (e.g., average temperatures in regions, the tropopause height) and for geographical reasons (e.g., moisture from the Gulf of Mexico). For example, Figure A2 presents the BTs of the ABI IR12.3 channel for (a) the region of higher GLM DE and (b) the region of lower GLM DE. Brightness temperatures (BTs) are one average about 2 K colder in Figure A2(a) than in Figure A2(b), meaning the CTs reach higher altitudes. Figure A3 compares the WV6.2 channel for the region of (a) higher and (b) lower GLM DE. Again, the BTs in the region of higher GLM DE are about 2 K colder than in the region of lower GLM DE. The water vapor channel gets saturated at higher altitudes in the region of higher GLM DE as the atmosphere contains in general more moisture than in the region of lower GLM DE. The WV7.3 channel results confirm this finding for the mid-level water vapor (not shown). These differences can be observed throughout all the thunderstorm categories (Table 3) and, thus, they are independent of the LJ/LD detection. A detailed analysis of the thunderstorm categories withLJ and withLD in the two regions confirmed that the thunderstorms with LJs and those with LDs, respectively, feature similar characterisitics when the

https://doi.org/10.5194/egusphere-2024-174
Preprint. Discussion started: 12 February 2024

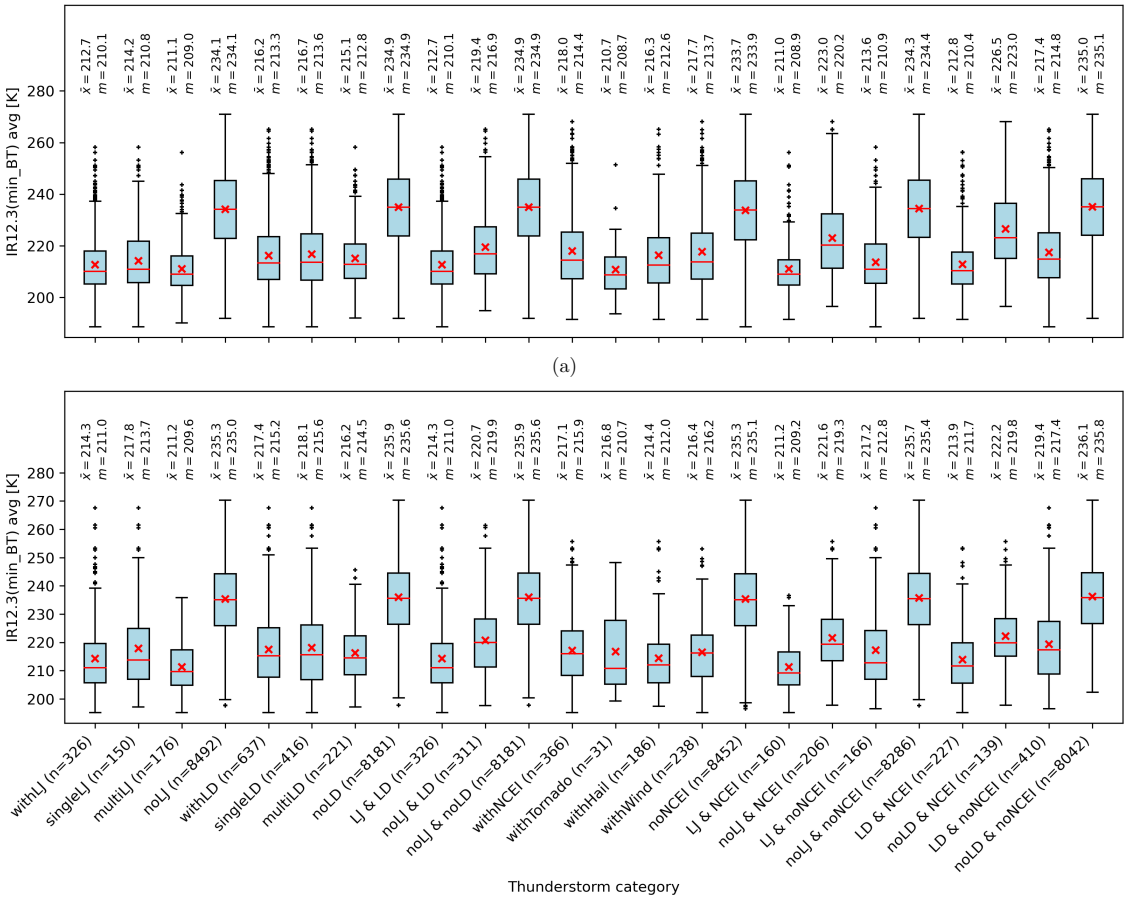

Figure A2. Trajectory minimum over cell-averaged BTs of the IR12.3 ABI channel for the region with (a) higher and (b) lower GLM DE. $\bar{x}$ shows the mean, m the median for each thunderstorm category.

climatology bias is corrected. Small differences could be observed for the OTs, that are slightly more frequent and stronger in the region of lower GLM DE for thunderstorms with LJs and/or LDs. The thunderstorms in the region of higher GLM DE are on average smaller than in the region of lower GLM DE, indicating that the storm types differ and there are likely more single-cell, thermally driven thunderstorms in the southeast than further north in the CONUS.

A3 Appendix Conclusion

LJ and LD detection are slightly influenced by the differences in the GLM flash DE. For example, detection algorithms could apply higher FR thresholds to slightly reduce the number of false alarms in the region of higher GLM DE. Nevertheless, the overall CSI skill remains comparable in both regions, as fewer hits are generated when applying higher FR thresholds. Hence, LJs and LDs can be detected using the same algorithm type over the entire central and eastern CONUS without a significant

https://doi.org/10.5194/egusphere-2024-174
Preprint. Discussion started: 12 February 2024

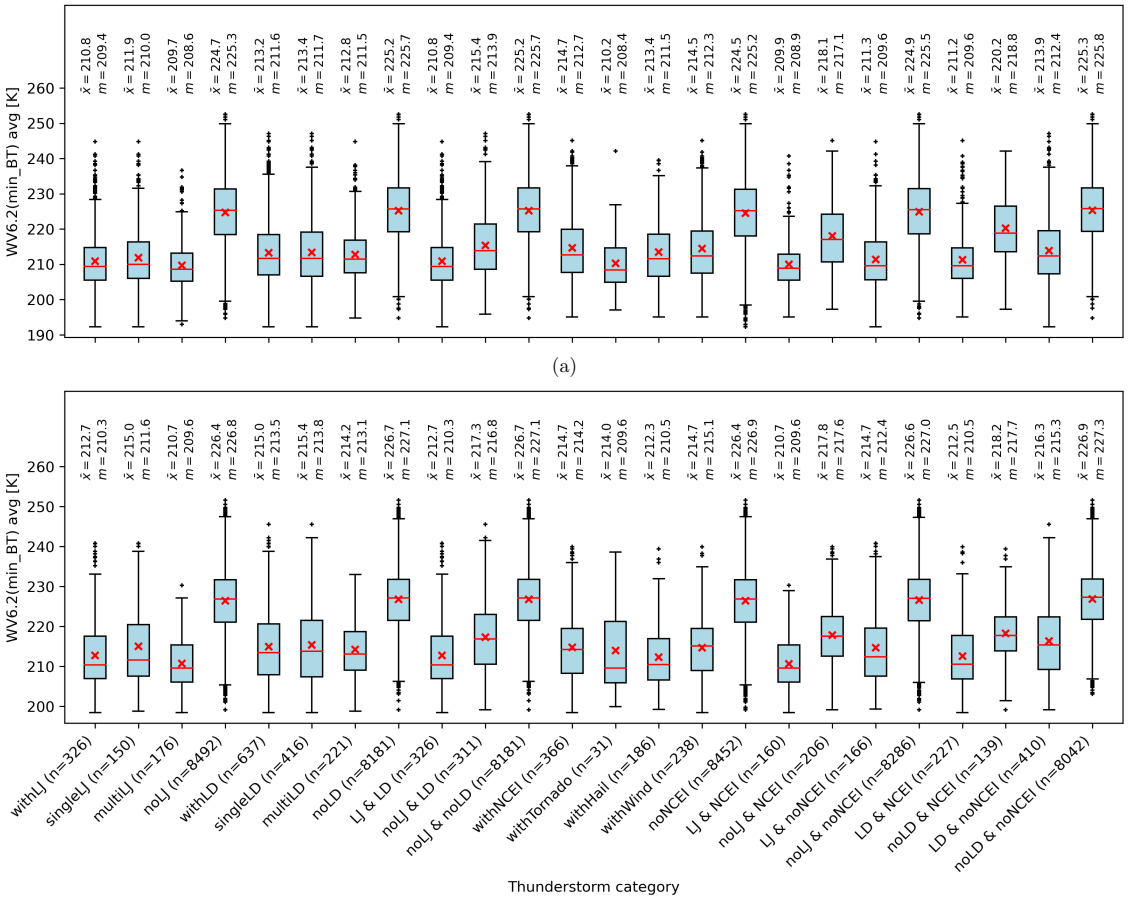

(a)

(b)

Figure A3. As Figure A2 but for BTs of the WV6.2 ABI channel.

impact on the algorithm performance. The thunderstorm characteristics vary slightly in the regions, with the differences being mainly attributed to the different climate and weather conditions in the southeastern and the remaining CONUS. Storms with LJs and/or LDs show the same trends as the other thunderstorm categories (i.e., thunderstorms without LJs and LDs) when comparing the results in the regions of higher and lower GLM DE.

Author contributions. FE wrote the paper text and created the figures. DRP was involved in content creation and internally reviewed the paper prior to submission. Both contributed to the journal peer review process.

Competing interests. The authors declare that they have no conflict of interest.

https://doi.org/10.5194/egusphere-2024-174
Preprint. Discussion started: 12 February 2024

Acknowledgements. The work of FE was supported by the fellowship "Towards an automated severe weather warning tool based on MTG-LI and FCI data" from the European Organisation for the Exploitation of Meteorological Satellites (EUMETSAT). The hosting institution of this fellowship is the Royal Meteorological Institute of Belgium (RMIB). The authors thank F. Autones, M. Claudon, and J.-M. Moisselin for providing, before a official release, the NWCSAF software package with included GLM data reader and their expertise on the RDT-CW package. The authors thank N. Clerbaux for setting up the new software version of NWCSAF at the RMIB and for downloading necessary satellite data. The authors acknowledge ECNWF for providing the necessary NWP data.

https://doi.org/10.5194/egusphere-2024-174
Preprint. Discussion started: 12 February 2024

References

Autones, F., Claudon, M., and Moisselin, J.-M.: Algorithm Theoretical Basis Document for the Convection Product Processors of the NWC/-GEO, Tech. Rep. version 2.2, Météo France, code NWC-CDOP2-GEO-MFT-SCI-ATBD-Convection, avalaible on nwcsaf.org, 2020.

Bateman, M., Mach, D., and Stock, M.: Further Investigation Into Detection Efficiency and False Alarm Rate for the Geostationary Lightning Mappers Aboard GOES-16 and GOES-17, Earth and Space Science, 8, e2020EA001 237, https://doi.org/https://doi.org/10.1029/2020EA001237, e2020EA001237 2020EA001237, 2021.

Blakeslee, R. J., Lang, T. J., Koshak, W. J., Buechler, D., Gatlin, P., Mach, D. M., Stano, G. T., Virts, K. S., Walker, T. D., Cecil, D. J., Ellett, W., Goodman, S. J., Harrison, S., Hawkins, D. L., Heumesser, M., Lin, H., Maskey, M., Schultz, C. J., Stewart, M., Bateman, M., Chanrion, O., and Christian, H.: Three Years of the Lightning Imaging Sensor Onboard the International Space Station: Expanded Global Coverage and Enhanced Applications, Journal of Geophysical Research: Atmospheres, 125, e2020JD032 918, https://doi.org/10.1029/2020JD032918, e2020JD032918 2020JD032918, 2020.

Borque, P., Vidal, L., Rugna, M., Lang, T. J., Nicora, M. G., and Nesbitt, S. W.: Distinctive Signals in 1-min Observations of Overshooting Tops and Lightning Activity in a Severe Supercell Thunderstorm, Journal of Geophysical Research: Atmospheres, 125, e2020JD032 856, https://doi.org/https://doi.org/10.1029/2020JD032856, e2020JD032856 2020JD032856, 2020.

Bourscheidt, V. and Ramos, M.-H.: On the Use of Geostationary Lightning Mapper Data as a Proxy for Precipitation, SSRN, https://doi.org/0.2139/ssrn.4594358, preprint, 2023.

Bruning, E. C., Tillier, C. E., Edgington, S. F., Rudlosky, S. D., Zajic, J., Gravelle, C., Foster, M., Calhoun, K. M., Campbell, P. A., Stano, G. T., Schultz, C. J., and Meyer, T. C.: Meteorological Imagery for the Geostationary Lightning Mapper, Journal of Geophysical Research: Atmospheres, 124, 14 285–14 309, https://doi.org/10.1029/2019JD030874, 10.1029/2019JD030874, 2019.

Chinchay, J. H. H.: Algorithm for Automatic Nowcasting Using ABI and GLM Data, in: 103rd AMS Annual Meeting, AMS, 2023.

Chronis, T., Carey, L. D., Schultz, C. J., Schultz, E. V., Calhoun, K. M., and Goodman, S. J.: Exploring lightning jump characteristics, Weather and Forecasting, 30, 23–37, https://doi.org/10.1175/WAF-D-14-00064.1, 2015.

Cintineo, J. L., Pavolonis, M. J., and Sieglaff, J. M.: ProbSevere LightningCast: A Deep-Learning Model for Satellite-Based Lightning Nowcasting, Weather and Forecasting, 37, 1239 – 1257, https://doi.org/https://doi.org/10.1175/WAF-D-22-0019.1, 2022.

Cummins, K. L.: On the Spatial and Temporal Variation of GLM Flash Detection and How to Manage It, 101st AMS Annual Meeting, virtual, 10-15 January 2021, extended abstract (personal communication Christoph J. Schultz) and presentation (https://ams.confex.com/ams/101ANNUAL/meetingapp.cgi/Paper/382589), 2021.

Curtis, N., Carey, L. D., and Schultz, C.: An Analysis of the Lightning Jump Algorithm Using Geostationary Lightning Mapper Flashes, in: 25th Int. Lightning Detection Conf./Seventh Int. Lightning Meteorology Conf., NASA, Fort Lauderdale, FL, 6 pp., 2018.

Deierling, W. and Petersen, W. A.: Total lightning activity as an indicator of updraft characteristics, J. Geophys. Res., 113, D16 210, 2008.

Dobber, M. and Grandell, J.: Meteosat Third Generation (MTG) Lightning Imager (LI) instrument performance and calibration from user perspective, Proc. 23rd Conf. on Characterization and Radiometric Calibration for Remote Sensing (CALCON), Logan, UT, Utah State University, 13 pp., 2014.

Erdmann, F.: Préparation à l'utilisation des observations de l'imageur d'éclairs de Météosat Troisième Génération pour la prévision numérique à courte échéance (Preparation for the use of Meteosat Third Generation Lightning Imager observations in short-term numerical weather prediction), Ph.D. thesis, Université Toulouse 3 – Paul Sabatier, Toulouse, France, 2020.

https://doi.org/10.5194/egusphere-2024-174
Preprint. Discussion started: 12 February 2024

Erdmann, F. and Poelman, D. R.: Automated Lightning Jump (LJ) Detection from Geostationary Satellite Data, Journal of Applied Meteorology and Climatology, 62, 1573 – 1590, https://doi.org/https://doi.org/10.1175/JAMC-D-22-0144.1, 2023.

EUMETSAT: Flexible Combined Imager (FCI), last accessed Nov 17, 2023, 5:02pm UTC, https://www.eumetsat.int/mtg-flexible-combined-imager-fci, 2021a.

EUMETSAT: Lightning Imager, last accessed Nov 17, 2023, 5:02pm UTC, https://www.eumetsat.int/mtg-lightning-imager, 2021b.

EUMETSAT: NWCSAF General Information, last accessed 08 Mar 2022, 7:32am UTC, https://www.nwcsaf.org/web/guest/nwcsaf-general-information, 2022.

Farnell, C. and Rigo, T.: The Lightning Jump Algorithm for Nowcasting Convective Rainfall in Catalonia, Atmosphere, 11, https://doi.org/10.3390/atmos11040397, 2020.

García-Pereda, J. and coauthors: Use of NWCSAF NWC/GEO software package with MSG, Himawari-8/9 and GOES-13/16 satellites, in: 2019 Joint EUMETSAT/AMS/NOAA Conference, Boston, USA, 2019.

Gatlin, P. N. and Goodman, S. J.: A total lightning trending algorithm to identify severe thunderstorms, Journal of Atmospheric and Oceanic Technology, 27, 3 – 22, https://doi.org/10.1175/2009JTECHA1286.1, 2010.

Goodman, S. J., Christian, H. J., and Rust, W. D.: A Comparison of the Optical Pulse Characteristics of Intracloud and Cloud-to-Ground Lightning as Observed above Clouds, Journal of Applied Meteorology, 27(12), 1369–1381, https://doi.org/10.1175/1520-0450(1988)027<1369:ACOTOP>2.0.CO;2, 1988.

Goodman, S. J., Blakeslee, R. J., Koshak, W. J., Mach, D., Bailey, J., Buechler, D., Carey, L., Schultz, C., Bateman, M., McCaul, E., and Stano, G.: The GOES-R Geostationary Lightning Mapper (GLM), Atmospheric Research, 125-126, 34 – 49, https://doi.org/10.1016/j.atmosres.2013.01.006, 2013.

Lang, T. J., Ávila, E. E., Blakeslee, R. J., Burchfield, J., Wingo, M., Bitzer, P. M., Carey, L. D., Deierling, W., Goodman, S. J., Medina, B. L., Melo, G., and Pereyra, R. G.: The RELAMPAGO Lightning Mapping Array: Overview and Initial Comparison with the Geostationary Lightning Mapper, Journal of Atmospheric and Oceanic Technology, 2020.

Leinonen, J., Hamann, U., Germann, U., and Mecikalski, J. R.: Nowcasting thunderstorm hazards using machine learning: the impact of data sources on performance, Natural Hazards and Earth System Sciences, 22, 577–597, https://doi.org/10.5194/nhess-22-577-2022, 2022.

MacGorman, D. R. and Rust, W. D.: The electrical nature of storms, Oxford University Press, 198 Madison Avenue, New York, New York 10016, 1 edn., ISBN 0-19-507337-1, 1998.

Mach, D. M.: Geostationary Lightning Mapper Clustering Algorithm Stability, Journal of Geophysical Research: Atmospheres, 125, e2019JD031 900, https://doi.org/10.1029/2019JD031900, e2019JD031900 2019JD031900, 2020.

Marchand, M., Hilburn, K., and Miller, S. D.: Geostationary Lightning Mapper and Earth Networks Lightning Detection Over the Contiguous United States and Dependence on Flash Characteristics, Journal of Geophysical Research: Atmospheres, 124, 11 552–11 567, https://doi.org/10.1029/2019JD031039, 2019JD031039, 2019.

Mikuš Jurković, P., Mahović, N. S., and Počakal, D.: Lightning, overshooting top and hail characteristics for strong convective storms in Central Europe, Atmospheric Research, 161-162, 153–168, https://doi.org/https://doi.org/10.1016/j.atmosres.2015.03.020, 2015.

Murphy, M. J. and Said, R. K.: Comparisons of Lightning Rates and Properties From the U.S. National Lightning Detection Network (NLDN) and GLD360 With GOES-16 Geostationary Lightning Mapper and Advanced Baseline Imager Data, Journal of Geophysical Research: Atmospheres, 125, e2019JD031 172, https://doi.org/10.1029/2019JD031172, e2019JD031172 2019JD031172, 2020.

NASA: Instruments: Advanced Baseline Imager (ABI), last accessed Mar 24, 2022, 5:02pm UTC, https://www.goes-r.gov/spacesegment/abi.html, 2022.

https://doi.org/10.5194/egusphere-2024-174
Preprint. Discussion started: 12 February 2024

NCEI-NOAA: The National Centers for Environmental Information (NCEI) storm events database, last accessed on 04 Jan 2023, https://www.ncdc.noaa.gov/stormevents/, 2020.

Ni, X., Huang, F., Hui, W., and Xiao, H.: Lightning Evolution in Hailstorms From the Geostationary Lightning Mapper Over the Contiguous United States, Journal of Geophysical Research: Atmospheres, 128, e2023JD038 578, https://doi.org/https://doi.org/10.1029/2023JD038578, e2023JD038578 2023JD038578, 2023.

Nisi, L., Hering, A., Germann, U., Schroeer, K., Barras, H., Kunz, M., and Martius, O.: Hailstorms in the Alpine region: Diurnal cycle, 4D-characteristics, and the nowcasting potential of lightning properties, Quarterly Journal of the Royal Meteorological Society, 146, 4170–4194, https://doi.org/https://doi.org/10.1002/qj.3897, 2020.

Pandit, S., Mishra, S., Mittal, A., and Devrani, A. K.: Nowcasting severity of thunderstorm associated with strong wind flow over Indian Subcontinent: Resource lightning surge, Atmósfera, 37, 85–98, https://doi.org/10.20937/ATM.53042, 2023.

Rigo, T. and Farnell, C.: Characterisation of Thunderstorms with Multiple Lightning Jumps, Atmosphere, 13, https://doi.org/10.3390/atmos13020171, 2022.

Rudlosky, S. D. and Fuelberg, H. E.: Documenting Storm Severity in the Mid-Atlantic Region Using Lightning and Radar Information, Monthly Weather Review, 141, 3186–3202, https://doi.org/10.1175/MWR-D-12-00287.1, 2013.

Schultz, C. J., Petersen, W. A., and Carey, L. D.: Preliminary Development and Evaluation of Lightning Jump Algorithms for the Real-Time Detection of Severe Weather, Journal of Applied Meteorology and Climatology, 48, 2543 – 2563, https://doi.org/10.1175/2009JAMC2237.1, 2009.

Schultz, C. J., Petersen, W. A., and Carey, L. D.: Lightning and Severe Weather: A Comparison between Total and Cloud-to-Ground Lightning Trends, Weather and Forecasting, 26, 744–755, https://doi.org/10.1175/WAF-D-10-05026.1, 2011.

Schultz, C. J., Carey, L. D., Schultz, E. V., and Blakeslee, R. J.: Kinematic and Microphysical Significance of Lightning Jumps versus Non-jump Increases in Total Flash Rate, Weather and Forecasting, 32, 275 – 288, https://doi.org/https://doi.org/10.1175/WAF-D-15-0175.1, 2017.

Schultz, E. V., Schultz, C. J., Carey, L. D., Cecil, D. J., and Bateman, M.: Automated Storm Tracking and the Lightning Jump Algorithm Using GOES-R Geostationary Lightning Mapper (GLM) Proxy Data, Journal of Operational Meteorology, 4(7), 92–107, https://doi.org/10.15191/nwajom.2016.0407, 2016.

scikit-learn developers: sklearn.cluster.DBSCAN, last accessed on 11 Mar 2022, 4:44pm UTC, https://scikit-learn.org/stable/modules/generated/sklearn.cluster.DBSCAN.html, 2007-2022.

Steiger, S. M., Orville, R. E., and Carey, L. D.: Total Lightning Signatures of Thunderstorm Intensity over North Texas. Part I: Supercells, Monthly Weather Review, 135, 3281–3302, https://doi.org/10.1175/MWR3472.1, 2007a.

Steiger, S. M., Orville, R. E., and Carey, L. D.: Total Lightning Signatures of Thunderstorm Intensity over North Texas. Part II: Mesoscale Convective Systems, Monthly Weather Review, 135, 3303–3324, https://doi.org/10.1175/MWR3483.1, 2007b.

Stough, S. M., Carey, L. D., Schultz, C. J., and Bitzer, P. M.: Investigating the Relationship between Lightning and Mesocyclonic Rotation in Supercell Thunderstorms, Weather and Forecasting, 32, 2237 – 2259, https://doi.org/10.1175/WAF-D-17-0025.1, 2017.

Thiel, K. C., Calhoun, K. M., Reinhart, A. E., and MacGorman, D. R.: GLM and ABI Characteristics of Severe and Convective Storms, Journal of Geophysical Research: Atmospheres, 125, e2020JD032 858, https://doi.org/https://doi.org/10.1029/2020JD032858, e2020JD032858 10.1029/2020JD032858, 2020.

Wapler, K.: The life-cycle of hailstorms: Lightning, radar reflectivity and rotation characteristics, Atmospheric Research, 193, 60–72, https://doi.org/https://doi.org/10.1016/j.atmosres.2017.04.009, 2017.

https://doi.org/10.5194/egusphere-2024-174
Preprint. Discussion started: 12 February 2024

Williams, E., Boldi, B., Matlin, A., Weber, M., Hodanish, S., Sharp, D., Goodman, S., Raghavan, R., and Buechler, D.: The behavior of total lightning activity in severe Florida thunderstorms, Atmospheric Research, 51, 245 – 265, https://doi.org/10.1016/S0169-8095(99)00011-3, 1999.

Wu, F., Cui, X., and Zhang, D.-L.: A lightning-based nowcast-warning approach for short-duration rainfall events: Development and testing over Beijing during the warm seasons of 2006–2007, Atmospheric Research, 205, 2–17, https://doi.org/https://doi.org/10.1016/j.atmosres.2018.02.003, 2018.

Zhang, D. and Cummins, K. L.: Time Evolution of Satellite-Based Optical Properties in Lightning Flashes, and its Impact on GLM Flash Detection, Journal of Geophysical Research: Atmospheres, 125, e2019JD032 024, https://doi.org/10.1029/2019JD032024, e2019JD032024 2019JD032024, 2020.